

PREPARATION AND CHARACTERIZATION OF MANGANESE-BASED AND
CARBON-BASED NANOMATERIALS FOR SUPERCAPACITORS APPLICATION

GOMAA ABDELGAWAD MOHAMMED ALI

Thesis submitted in fulfillment of the requirements for the award of the degree of
Doctor of Philosophy (Advanced Materials)

Faculty of Industrial Science and Technology

UNIVERSITI MALAYSIA PAHANG

July 2015

ABSTRACT

In this study, electrochemical materials, namely MnO₂, reduced graphene oxide (rGO), porous carbon nanoparticles (PCNs), and rGO/MnO₂ nanocomposite, were prepared in diverse morphologies such as nanoflowers (MnO₂), nanosheets (rGO), and nanoparticles (carbon). Different physical and chemical characterizations have been conducted to study the structural and morphological properties of the materials under study. Electrochemical properties of the above materials have been studied comprehensively using cyclic voltammetry (CV), galvanostatic charge–discharge (CDC) and electrochemical impedance spectroscopy (EIS) in order to evaluate their suitability as an electrode for supercapacitive energy storage. MnO₂ nanoflowers were recovered from spent batteries by a combining leaching and electrowinning techniques. The recovered MnO₂ nanoflowers exhibited high specific capacitance (C_s) (303 F g⁻¹ at 5 mV s⁻¹). Furthermore, MnO₂ was electrodeposited by potentiostatic and galvanostatic conditions. Under similar electrodeposition conditions, MnO₂ deposited by galvanostatic condition showed smaller particle size, less compact layered structure and wider band gap compared to potentiostatic deposition. The galvanostatic MnO₂ rendered facile ions diffusion, low resistances and showed superior capacitive behavior. The rGO nanosheets were prepared by hydrazine reduction of graphene oxide and their electrochemical properties were studied. The rGO showed high C_s of 191 and 168 F g⁻¹ at 5 mV s⁻¹, in 5 M KOH and 1 M Na₂SO₄, respectively and high cycling stability > 96 % over 1000 cycles. In addition, PCNs with fine particles size of 35 nm were prepared from oil palm leaves using a catalyst free process. The C_s of PCNs is 245 and 213 F g⁻¹ at 5 mV s⁻¹ in 5 M KOH and 1 M Na₂SO₄, respectively. The PCNs showed high cycling stability of 95 %. Practical supercapacitors were developed using rGO and PCNs; the devices delivered energy densities ~18 and ~25 W h kg⁻¹ at power densities 340 and 360 W kg⁻¹, respectively, under wider operating voltage window of 2 V in neutral electrolyte. rGO/MnO₂ nanocomposite has been prepared by simultaneous electrochemical conversion of GO and Mn₃O₄. The C_s of rGO/MnO₂ is 457 F g⁻¹ at 5 mV s⁻¹, which are several folds higher compared to those for pure rGO and MnO₂. Furthermore, rGO/MnO₂ showed high stability of 95 % over 2000 CDC cycles. Therefore, the present study identifies electrochemical materials with improved energy storage capabilities.

ABSTRAK

Dalam kajian ini, bahan electrokimia iaitu MnO_2 , graphene oksida terturun (rGO), karbon nanopartikel berongga (PCNs), dan rGO/ MnO_2 nanokomposit telah disediakan in pelbagai morfologi, seperti nanobunga (MnO_2), nanolembaran (rGO), dan nanopartikel (karbon). Pelbagai ujian sifat fizikal dan sifat kimia yang berbeza telah dijalankan untuk memahami struktur dan morfologi bahan yang dikaji. Sifat electrokimia telah dikaji secara menyeluruh dengan menggunakan kaedah siklik voltammetrik (CV), galvanostatik cas-discas (CDC) dan electrokimia impedans spektroskopi (EIS) demi menilai kesesuaian sebagai elektrod dalam penyimpanan tenaga superkapasitif. MnO_2 nanobunga telah didapati kembali daripada bateri terpakai dengan kombinasi kaedah larut lesap dan *electrowinning*. MnO_2 nanobunga yang didapati kembali menunjukkan kapasitans spesifik (C_s) (303 F g^{-1} at 5 mV s^{-1}). Tambahan, MnO_2 juga dielektrodeposit dengan kaedah potentiostatik dan galvanostatik. Untuk keadaan proses electrodeposit yang sama, MnO_2 yang dideposit dengan kaedah galvanostatik menunjukkan partikel saiz yang lebih kecil, kepadatan struktur yang rendah dan jurang jalur yang lebih lebar berbanding dengan kaedah potentiostatik. MnO_2 yang dihasilkan melalui kaedah galvanostatik membenarkan resapan ion yang mudah, rintangan yang rendah dan menunjukkan sifat kapasiti yang lebih baik. rGO nanolembaran telah disediakan melalui penurunan graphene oksida dengan hydrazine dan sifat electrokimia telah dikaji. rGO menunjukkan C_s yang tinggi iaitu 191 dan 168 F g^{-1} pada 5 mV s^{-1} , di dalam 5 M KOH dan $1 \text{ M Na}_2\text{SO}_4$, masing-masing dan kestabilan kitaran yang tinggi $> 96 \%$ untuk 1000 kitaran. Tambahan, PCNs dengan partikel saiz yang halus 35 nm turut disediakan dengan daun kelapa sawit tanpa menggunakan pemangkin. C_s untuk PCNs adalah 245 dan 213 F g^{-1} pada 5 mV s^{-1} di dalam 5 M KOH dan $1 \text{ M Na}_2\text{SO}_4$, masing-masing. PCNs menunjukkan kestabilan kitaran yang tinggi 95% . Superkapasitor praktikal telah disediakan dengan menggunakan rGO dan PCNs dan peranti tersebut menghasilkan tenaga ~ 18 dan $\sim 25 \text{ W h kg}^{-1}$ pada kuasa 340 and 360 W kg^{-1} , masing-masing, di bawah operasi voltan 2 V di dalam neutral elektrolit. rGO/ MnO_2 nanokomposit telah disediakan dengan kaedah pertukaran electrokimia GO dan Mn_3O_4 . C_s untuk rGO/ MnO_2 adalah 457 F g^{-1} pada 5 mV s^{-1} dan nilai ini adalah beberapa kali ganda lebih tinggi berbanding dengan rGO dan MnO_2 tulen. Tambahan, rGO/ MnO_2 menunjukkan kestabilan tinggi 95% untuk 2000 kitaran CDC. Oleh demikian, kajian ini menunjukkan bahan electrokimia yang mempunyai keupayaan simpan tenaga yang ditambahbaikkan.

TABLE OF CONTENTS

| | |
|---------------------------------|-------|
| SUPERVISOR'S DECLARATION | ii |
| STUDENT'S DECLARATION | iii |
| ACKNOWLEDGEMENT | v |
| ABSTRACT | vi |
| ABSTRAK | vii |
| TABLE OF CONTENTS | viii |
| LIST OF TABLES | xiv |
| LIST OF FIGURES | xv |
| LIST OF SYMBOLS | xviii |
| LIST OF ABBREVIATIONS | xxi |

CHAPTER 1 INTRODUCTION

| | |
|--------------------------------|---|
| 1.1 Chapter Overview | 1 |
| 1.2 Background and Motivations | 1 |
| 1.3 Problem Statement | 3 |
| 1.4 Objectives of Research | 5 |
| 1.5 Scope of the Thesis | 5 |
| 1.6 Thesis Outlines | 6 |

CHAPTER 2 LITERATURE REVIEW

| | |
|---|----|
| 2.1 Chapter Overview | 7 |
| 2.2 Electrochemical Capacitors | 7 |
| 2.3 Supercapacitors, Batteries and Fuel Cells | 8 |
| 2.4 Supercapacitors Applications | 9 |
| 2.5 Energy Storage Mechanisms | 10 |
| 2.6 Supercapacitors Components | 13 |
| 2.6.1 Electrode Materials | 13 |
| 2.6.2 Electrolytes | 19 |
| 2.6.3 Separators | 20 |
| 2.7 Supercapacitors Cell Assembly | 20 |
| 2.8 Conclusions | 21 |

CHAPTER 3 EXPERIMENTAL PROCEDURES AND TECHNIQUES

| | |
|---|----|
| 3.1 Chapter Overview | 22 |
| 3.2 Samples Preparation Procedures | 22 |
| 3.2.1 Preparation of MnO ₂ from Recycling of Spent Batteries | 22 |
| 3.2.2 Preparation of MnO ₂ by Potentiostatic and Galvanostatic Electrodeposition | 24 |
| 3.2.3 Preparation of Reduced Graphene Oxide Nanosheets | 24 |
| 3.2.4 Preparation of Carbon Nanoparticles from Biowaste | 25 |

| | |
|--|----|
| 3.2.5 Preparation of Reduced Graphene Oxide/MnO ₂ Nanocomposite | 25 |
| 3.3 Sample Characterization Techniques | 27 |
| 3.3.1 X-Ray Diffraction | 27 |
| 3.3.2 Fourier Transformed Infrared Spectrometry | 28 |
| 3.3.3 Thermal Analysis | 29 |
| 3.3.4 N ₂ Adsorption–Desorption Isotherms | 29 |
| 3.3.5 Ultraviolet–Visible Spectroscopy | 30 |
| 3.3.6 Raman Spectra | 31 |
| 3.3.7 Field Emission Scanning Electron Microscopy | 31 |
| 3.3.8 Transmission Electron Microscopy | 32 |
| 3.4 Electrodes Preparation and Cells Setup | 33 |
| 3.5 Specific Capacitance and other Electrochemical Parameters Calculations | 34 |
| 3.6 Summary | 36 |

CHAPTER 4 SYNTHESIS AND CHARACTERIZATION OF MnO₂ AS SUPERCAPACITOR ELECTRODE

| | |
|---|----|
| 4.1 Chapter Overview | 37 |
| 4.2 Introduction | 37 |
| 4.3 Results and Discussion | 39 |
| 4.3.1 Structural and Morphological Analyses | 39 |
| 4.3.2 Optical Band Gaps | 43 |
| 4.3.3 Electrochemical Studies | 44 |

| | |
|-----------------|----|
| 4.4 Conclusions | 53 |
|-----------------|----|

CHAPTER 5 SYNTHESIS AND CHARACTERIZATION OF REDUCED GRAPHENE Oxide NANOSHEETS AS SUPERCAPACITOR ELECTRODE

| | |
|--|----|
| 5.1 Chapter Overview | 54 |
| 5.2 Introduction | 54 |
| 5.3 Results and Discussion | 55 |
| 5.3.1 Structural and Morphological Analyses | 55 |
| 5.3.2 Electrochemical Studies of rGONS | 60 |
| 5.3.3 Electrochemical Properties of rGONS//rGONS | 67 |
| 5.4 Conclusions | 71 |

CHAPTER 6 SYNTHESIS AND CHARACTERIZATION OF POROUS CARBON NANOPARTICLES AS SUPERCAPACITOR ELECTRODE

| | |
|---|----|
| 6.1 Chapter Overview | 72 |
| 6.2 Introduction | 72 |
| 6.3 Results and Discussion | 73 |
| 6.3.1 Structural and Morphological Analyses | 73 |
| 6.3.2 Electrochemical Studies of PCNs | 75 |
| 6.3.3 Electrochemical Studies of PCNs//PCNs | 80 |
| 6.4 Conclusions | 84 |

CHAPTER 7 SYNTHESIS AND CHARACTERIZATION OF REDUCED GRAPHENE OXIDE/MnO₂ NANOCOMPOSITE AS SUPERCAPACITOR ELECTRODE

| | |
|---|----|
| 7.1 Chapter Overview | 85 |
| 7.2 Introduction | 85 |
| 7.3 Results and Discussion | 87 |
| 7.3.1 Structural and Morphological Analyses | 87 |
| 7.3.2 Electrochemical Studies | 93 |
| 7.4 Conclusions | 99 |

CHAPTER 8 CONCLUSIONS AND RECOMMENDATIONS

| | |
|---|-----|
| 8.1 Introduction | 100 |
| 8.2 Conclusions | 100 |
| 8.2.1 Structural and Morphological Properties | 100 |
| 8.2.2 Electrochemical Properties | 101 |
| 8.3 Recommendations for Future Research | 103 |

| | |
|---------------------|-----|
| ACHIEVEMENTS | 105 |
|---------------------|-----|

| | |
|-------------------|-----|
| REFERENCES | 109 |
|-------------------|-----|

LIST OF TABLES

| Table No. | Title | Page No. |
|-------------------|--|-----------------|
| Table 4.1: | Fitting parameters of the experimental impedance data for MnO ₂ (GS), MnO ₂ (Bt) and MnO ₂ (PS) | 53 |
| Table 5.1: | Fitting parameters of the experimental impedance data for rGONS in 5 M KOH and 1 M Na ₂ SO ₄ electrolytes | 66 |
| Table 6.1: | Fitting parameters of the experimental impedance data for PCNs in 5 M KOH and 1 M Na ₂ SO ₄ electrolytes | 79 |
| Table 7.1: | Comparison of reported specific capacitance with graphene and MnO ₂ based nanocomposites | 95 |
| Table 7.2: | Fitting parameters of the experimental impedance data for rGO(CV), MnO ₂ (CV), rGO/MnO ₂ (CV) | 99 |
| Table 8.1: | Comparison of the specific capacitance values and other electrochemical parameters for all materials under this study | 103 |

LIST OF FIGURES

| Figure No. | Title | Page No. |
|--------------------|---|----------|
| Figure 2.1: | Ragone plot of various energy storage systems (Winter and Brodd, 2004) | 9 |
| Figure 2.2: | Schematic diagrams of EDLCs in discharged (left) and charged (right) states (Chen and Dai, 2013) | 11 |
| Figure 2.3: | Cyclic voltammogram of electrochemical capacitors (Frackowiak and Béguin, 2001) | 13 |
| Figure 3.1: | Simple graphical representation of reduced graphene oxide/MnO ₂ nanocomposite preparation | 26 |
| Figure 3.2: | Scheme illustrating the Bragg's relation and example of XRD diffractogram | 28 |
| Figure 3.3: | Practical three-electrode system (left) and two-electrode system (right) used for supercapacitive measurements. | 34 |
| Figure 4.1: | XRD patterns of MnO ₂ (Bt), MnO ₂ (GS) and MnO ₂ (PS) | 39 |
| Figure 4.2: | FTIR spectra of MnO ₂ (Bt), MnO ₂ (GS) and MnO ₂ (PS) | 40 |
| Figure 4.3: | FESEM images of (a) MnO ₂ (Bt), (c) MnO ₂ (GS) and (e) MnO ₂ (PS); (b), (d) and (f) are high magnifications of the same materials, respectively | 42 |
| Figure 4.4: | (a) UV-Vis spectra, (b) direct transition $(ah\nu)^2$ versus $h\nu$ and (c) indirect transition $(ah\nu)^{1/2}$ versus $h\nu$ curves for MnO ₂ (Bt), MnO ₂ (GS) and MnO ₂ (PS) | 44 |
| Figure 4.5: | Cyclic voltammetry curves of Ni foam at different scan rates in (a) 5 M KOH (-1 – 0) V, (b) 1 M Na ₂ SO ₄ (0 – 1) V, (c) 1 M Na ₂ SO ₄ (-1 – 0) V, the insets show the specific capacitance as a function of scan rate; and (d) galvanostatic charge-discharge curves at 0.5 A g ⁻¹ in both electrolytes | 45 |
| Figure 4.6: | Cyclic voltammograms at different scan rates for (a) MnO ₂ (Bt), (b) MnO ₂ (GS) and (c) MnO ₂ (PS); (d) variation of specific capacitance as a function of scan rate | 47 |

| | | |
|---------------------|--|----|
| Figure 4.7: | Galvanostatic charge–discharge curves at different current densities for (a) MnO ₂ (Bt), (b) MnO ₂ (GS) and (c) MnO ₂ (PS): (d) variation of specific capacitance as a function of discharge current density | 49 |
| Figure 4.8: | (a) Cycling stability and (b) MnO ₂ (Bt) Coulombic efficiency for MnO ₂ (Bt), MnO ₂ (GS) and MnO ₂ (PS): at 3 A g ⁻¹ in 1 M Na ₂ SO ₄ | 50 |
| Figure 4.9: | (a) Nyquist plots, the inset is the high–frequency region of the plots, (b) Bode plots, (c) real and (d) imaginary parts of the capacitance as function of the frequency for MnO ₂ (Bt), MnO ₂ (GS) and MnO ₂ (PS) | 52 |
| Figure 5.1: | (a) XRD patterns, (b) FTIR, (c) UV–Vis and (d) Raman spectra of GO and rGONS | 56 |
| Figure 5.2: | TGA and DTA curves for GO and rGONS | 58 |
| Figure 5.3: | N ₂ adsorption–desorption isotherms of GO and rGONS, the inset is the pore size distributions | 59 |
| Figure 5.4: | FESEM images of (a) GO and (b) rGONS, the inset of (b) shows high magnification image of rGONS | 60 |
| Figure 5.5: | Cyclic voltammetry curves in (a) 5 M KOH and (b) 1 M Na ₂ SO ₄ at different potential windows at 25 mV s ⁻¹ for rGONS | 61 |
| Figure 5.6: | Cyclic voltammetry curves (a) in 5 M KOH, (b) in 1 M Na ₂ SO ₄ at different scan rates, (c) at 25 mV s ⁻¹ and (d) variation of specific capacitance as a function of scan rate in both electrolytes for rGONS | 62 |
| Figure 5.7: | Galvanostatic charge–discharge curves (a) in 5 M KOH, (b) in 1 M Na ₂ SO ₄ at different current densities, (c) at 1 A g ⁻¹ and (d) specific capacitance of current density in both electrolytes for rGONS | 63 |
| Figure 5.8: | Cycling stability (left vs. bottom) and Coulombic efficiency (right vs. bottom) at 1 A g ⁻¹ in (a) 5 M KOH and (b) 1 M Na ₂ SO ₄ for rGONS | 64 |
| Figure 5.9: | (a) Nyquist plots, the inset is the high–frequency region of the plots, (b) Bode plots, (c) real and (d) imaginary parts of the capacitance as function of the frequency in 5 M KOH and 1 M Na ₂ SO ₄ for rGONS | 66 |
| Figure 5.10: | Cyclic voltammetry curves (a) in 5 M KOH, (b) in 1 M Na ₂ SO ₄ at different scan rates, (c) in 1 M Na ₂ SO ₄ under different potential windows at 25 mV s ⁻¹ : and (d) variation of specific capacitance as a function of scan rate in both electrolytes and all potential windows for rGONS//rGONS | 68 |

| | | |
|---------------------|---|----|
| Figure 5.11: | Galvanostatic charge–discharge curves (a) in 5 M KOH, (b) in 1 M Na ₂ SO ₄ at different current densities, (c) in 1 M Na ₂ SO ₄ under different potential windows at 0.5 A g ⁻¹ : and (d) variation of specific capacitance as a function of current density in both electrolytes and all potential windows for rGONS//rGONS | 69 |
| Figure 5.12: | Cycling stability (left vs. bottom) and Coulombic efficiency (right vs. bottom) at 1 A g ⁻¹ current density in (a) 5 M KOH and (b) 1 M Na ₂ SO ₄ for rGONS//rGONS | 70 |
| Figure 5.13: | Ragone plot for rGONS//rGONS in different electrolytes and voltage windows | 71 |
| Figure 6.1: | (a) XRD pattern, (b) FTIR spectra, (c) N ₂ adsorption–desorption isotherm and (d) Raman for PCNs | 74 |
| Figure 6.2: | (a) FESEM and (b) TEM images for PCNs | 75 |
| Figure 6.3: | Cyclic voltammetry curves (a) in 5 M KOH, (b) in 1 M Na ₂ SO ₄ , (c) at 25 mV s ⁻¹ and (d) variation of specific capacitance as a function of scan rate in both electrolytes for PCNs | 76 |
| Figure 6.4: | Galvanostatic charge–discharge curves (a) in 5 M KOH, (b) in 1 M Na ₂ SO ₄ at different current densities, (c) at 1 A g ⁻¹ and (d) variation of specific capacitance as a function of current density in both electrolytes for PCNs | 77 |
| Figure 6.5: | Cycling stability (left vs. bottom) and Coulombic efficiency (right vs. bottom) at 1 A g ⁻¹ in (a) 5 M KOH and (b) 1 M Na ₂ SO ₄ for PCNs | 78 |
| Figure 6.6: | (a) Nyquist plots, the inset is the high–frequency region of the plots, (b) Bode plots, (c) real and (d) imaginary parts of the capacitance as function of the frequency in 5 M KOH and 1 M Na ₂ SO ₄ for PCNs | 80 |
| Figure 6.7: | Cyclic voltammetry curves (a) in 5 M KOH, (b) in 1 M Na ₂ SO ₄ at different scan rates, (c) in 1 M Na ₂ SO ₄ under different potential windows at 25 mV s ⁻¹ : and (d) variation of specific capacitance as a function of scan rate in both electrolytes and all potential windows for PCNs//PCNs | 81 |
| Figure 6.8: | Galvanostatic charge–discharge curves (a) in 5 M KOH, in 1 M Na ₂ SO ₄ (0 – 1) V, (c) in 1 M Na ₂ SO ₄ (0 – 2) V at different current densities and (d) variation of specific capacitance as a function of current density in both electrolytes and all potential windows for PCNs//PCNs | 82 |
| Figure 6.9: | Cycling stability (left vs. bottom) and Coulombic efficiency (right vs. bottom) at 1 A g ⁻¹ current density in (a) 5 M KOH and (b) 1 M Na ₂ SO ₄ for PCNs//PCNs | 83 |

| | | |
|---------------------|---|----|
| Figure 6.10: | Ragone plot for PCNs//PCNs in different electrolytes and voltage windows | 84 |
| Figure 7.1: | (a) XRD patterns, (b) FTIR and (c) Raman spectra for rGO(CV), MnO ₂ (CV) and rGO/MnO ₂ (CV) | 88 |
| Figure 7.2: | (a) FESEM images for rGO(CV), (b) MnO ₂ (CV), (c) GO/Mn ₃ O ₄ and (d) rGO/MnO ₂ (CV): The inset of (d) is zoomed view of FESEM of rGO/MnO ₂ (CV) | 90 |
| Figure 7.3: | TEM images for (a) rGO(CV), (b) MnO ₂ (CV) and (c) rGO/MnO ₂ (CV) | 91 |
| Figure 7.4: | (a) UV–Vis spectra, (b) direct transition $(\alpha h\nu)^2$ versus $h\nu$ and (c) indirect transition $(\alpha h\nu)^{1/2}$ versus $h\nu$ curves for the rGO(CV), MnO ₂ (CV) and rGO/MnO ₂ (CV) | 92 |
| Figure 7.5: | (a) Cyclic voltammetry curves at different scan rates and (b) Galvanostatic charge–discharge curves at different current densities for rGO/MnO ₂ (CV) | 93 |
| Figure 7.6: | (a) Cyclic voltammetry curves at 25 mV s ⁻¹ , (b) variation of specific capacitance as a function of scan rate, (c) Galvanostatic charge–discharge curves at 1 A g ⁻¹ and (d) variation of specific capacitance as a function of current density for rGO(CV), MnO ₂ (CV) and rGO/MnO ₂ (CV) | 94 |
| Figure 7.7: | Cycling stability curve (left vs. bottom) and Columbic efficiency (right vs. bottom) at 3 A g ⁻¹ current density for rGO/MnO ₂ (CV) | 97 |
| Figure 7.8: | (a) Nyquist plots, the inset is the high–frequency region of the plots, (b) Bode plots, (c) real and (d) imaginary parts of the capacitance as function of the frequency for rGO(CV), MnO ₂ (CV) and rGO/MnO ₂ (CV) | 98 |

LIST OF SYMBOLS

| | |
|--------------|--|
| α | Absorption coefficient |
| C | Capacitance |
| Q | Charge |
| Δt_c | Charging time |
| η | Coulombic efficiency |
| B | Constant relative to the material |
| I | Current |
| $P_{SXR D}$ | Crystalline size |
| θ | Diffraction angle (degree) |
| Δt_d | Discharging time |
| S_E | Electrochemical active specific surface area |
| E_g | Energy band gap |
| E | Energy density |
| F | Farad |

| | |
|------------|--|
| f | Frequency |
| C'' | Imaginary part of the cell capacitance |
| Z'' | Imaginary part of the impedance |
| m | Mass of active material |
| M | Molar mass |
| n | Number of electrons |
| $h\nu$ | Photon energy |
| ΔV | Potential window |
| P | Power density |
| C' | Real part of the cell capacitance |
| Z' | Real part of the impedance |
| τ | Relaxation time |
| ν | Scan rate |
| k | Scherrer constant |

| | |
|-------------------|-------------------------------|
| C_s | Specific capacitance |
| C_{theo} | Theoretical pseudocapacitance |
| V | Volt |
| λ | Wavelength |

LIST OF ABBREVIATIONS

| | |
|-------|-------------------------------|
| 2D | Two Dimensional |
| 3D | Three Dimensional |
| 2ES | Two Electrode System |
| 3ES | Three Electrode System |
| AC | Activated Carbon |
| ASSCs | Asymmetric Supercapacitors |
| BET | Brunauer–Emmett–Teller |
| BJH | Barrett–Joyner–Halenda |
| CNTs | Carbon Nanotubes |
| CPE | Constant Phase Elements |
| CPs | Conducting Polymers |
| CV | Cyclic Voltammetry |
| DTA | Differential Thermal Analysis |
| DFT | Density Functional Theory |

| | |
|--------|---|
| ECs | Electrochemical Capacitors |
| EDL | Electrochemical Double Layer |
| EDLCs | Electrochemical Double Layer Capacitors |
| EIS | Electrochemical Impedance Spectroscopy |
| FESEM | Field Emission Scanning Electron Microscope |
| FTIR | Fourier Transform Infrared Spectroscopy |
| GO | Graphene Oxide |
| HCs | Hybrid Capacitors |
| JCPDS | Joint Committee on Powder Diffraction Standards |
| MWCNTs | Multi-Walled Carbon Nanotubes |
| OCP | Open Circuit Potential |
| OPL | Oil Palm Leaves |
| PANI | Polyaniline |
| PCs | Pseudocapacitors |

| | |
|--------|---|
| PCNs | Porous Carbon Nanoparticles |
| PBS | Phosphate Buffered Solution |
| PTFE | Polytetrafluoroethylene |
| rGO | Reduced Graphene Oxide |
| rGONS | Reduced Graphene Oxide Nanosheets |
| SSCs | Symmetric Supercapacitors |
| SWCNTs | Single-Walled Carbon Nanotubes |
| SWCNHs | Single-Walled Carbon Nanohorns |
| TEM | Transmission Electron Microscope |
| TGA | Thermogravimetric Analysis |
| UV-Vis | Ultraviolet-Visible Spectrophotometry |
| USEPA | United States Environmental Protection Agency |
| XRD | X-Ray Diffraction |
| Zn-C | Zinc-Carbon |

CHAPTER 1

INTRODUCTION

1.1 CHAPTER OVERVIEW

This chapter introduces the basic aspects about the materials used in this study and background for the energy storage properties of the materials. Motivation of the research, problem statement, research objectives and scope of work are also presented in this chapter.

1.2 BACKGROUND AND MOTIVATIONS

Electrochemical capacitors (ECs) are also known as ultracapacitors or supercapacitors. It can be classified into two main categories based on energy storage mechanism, pseudocapacitors (PCs) and electrochemical double-layer capacitors (EDLCs). PCs store electrical energy faradically by electron charge transfer between electrode and electrolyte. Metal oxides and conducting polymers are used as electrode materials for PCs. In EDLCs, a double layer of electrolyte ions is formed on the surface of an electrode material, which arises from the potential-dependence of the surface density of charges stored electrostatically. The electrode materials for EDLCs include all carbon-based materials. Supercapacitors could be used in many applications because of

their higher energy output as compared to conventional capacitors and higher power than batteries, in addition to their miniature size. Various types of electrode materials can be used in supercapacitors, including carbon-based materials, conducting polymers and metal oxides. In addition, the electrolyte could be an aqueous, organic or an ionic liquid. In case of an aqueous electrolyte, the operating voltage is limited to 1 V (due to the electrochemical decomposition of water at 1.23 V), whereas an organic electrolyte can achieve a voltage range of 2.5 to 3.5 V (Syzdek et al., 2014). A higher voltage of up to 4.0 V can be achieved for the ionic liquid. Supercapacitors have many advantages, for example, long life cycles, fast charging time, low impedance and high energy and power density, environmental friendly, and also can be operated in a wide temperature range. This study aims to investigate different materials for supercapacitor applications with high power and long life criteria for better energy storage devices. The energy storage properties are directly depending on the structure and morphology of the electrode materials.

In recent years, manganese dioxide (MnO_2) has drawn increasing attention for supercapacitors application, mainly due to the high abundance of manganese (Jang et al., 2012) that contributes to low material cost as compared to the expensive ruthenium metal. Pang et al. reported high specific capacitance (C_s) (700 F g^{-1}) for MnO_2 thin films in year 2000 and their findings had sparked strong interest among energy research community for its application in supercapacitor electrode (Pang and Anderson, 2000, Pang et al., 2000). Such high capacitance value arises from the ions insertion/desertion within MnO_2 structure and it depends crucially on the particle size, surface area and porosity. Since then, in achieving optimized condition for the aforementioned properties, MnO_2 with different morphologies have been developed, such as nanoflakes (Chou et al., 2006), nanorods (Yousefi et al., 2012a), nanowires (Yousefi et al., 2013), nanopetals (Yang et al., 2012) and nanosheets (Yan et al., 2012). The synthesis route plays a vital role in determining its morphology. The most common synthesis route for MnO_2 is chemical coprecipitation method (Deng et al., 2013, Jiang et al., 2009) involving dissolved Mn^{4+} precursor. However, instability of Mn^{4+} precursor in the aqueous solution as well as the contact resistance between synthesized MnO_2 and current collectors have hindered its wider use in electrochemical applications (Xu et al., 2008, Prasad and Miura, 2004).

Electrochemical deposition is proven to be an effective method to prepare MnO₂ nanostructures (Hu et al., 2014, Yousefi et al., 2013).

On the other hand, carbon-based materials possessing high surface area as the electrode material, and the capacitance originates from the charge accumulation at the interface between electrode and electrolyte (Portet et al., 2005). Pseudocapacitors employ transition metal oxides or conductive polymers (Patil et al., 2013, Song et al., 2013, Xie et al., 2012) as the electrode material. Though the energy densities in pseudocapacitors are higher than that of EDLCs, the faradic reactions within pseudocapacitors could lead to phase changes and limit their life time (Compton and Nguyen, 2010). Graphene with its high surface area and nanosheets morphology and carbon nanoparticles with porous structure are a promising materials from energy storage applications.

1.3 PROBLEM STATEMENT

The need for the development of efficient energy storage systems is paramount in meeting the world's future energy targets, especially when the energy costs are on the increase in addition to the escalating demand. Energy storage technologies can improve efficiencies in supply systems by storing the energy when it is in excess, and then release it timely. Nowadays, batteries are slowly becoming obsolete due to their poor cycleability (limited to a few thousands) and long charge time (tens of minutes) in comparison to supercapacitors. On the other hand, supercapacitors have long life time and fast charging times (Vangari et al., 2013). Nowadays the research focus on developed suitable electrode materials which directly reflect in supercapacitor technology enhancement.

MnO₂ has been identified as a promising pseudocapacitive material to replace toxic and costly materials especially ruthenium oxide. Though manganese source can be found abundantly in nature, it is imperative to stop exploiting nature for the advancement of technology. Instead, recovery of manganese from waste sources could be an alternative to obtain MnO₂. According to United States Environmental Protection Agency (USEPA) analysis, an average of 8 disposable batteries are consumed by an individual annually.

Annually, around 160 000 tonnes of batteries are placed on the market and around 20 000 tonnes per year of manganese could be recovered (Gallegos et al., 2013). Thus figures raise an alarm on the disposal issue where the common practice in handling spent batteries is landfill which could potentially harm the environment. Furthermore, high percentage of manganese in spent batteries could be a motivation in manganese recovery from batteries to be used as supercapacitor electrode (Sayilgan et al., 2009).

Carbon-based materials are the most widely used materials in commercial supercapacitor. However, activated carbon possesses the problem of achieving high C_s and thus limiting its wide application in supercapacitor. Graphene possesses high surface area, stable structure and exhibits many interesting electronic, optical and mechanical properties due to its 2D crystal structure. Graphene could be the solution for this problem. On the other hand, as a move to preserve the environment as well as maintain low cost material, waste precursors could be the potential source for the production of carbon-based materials. This include with oil palm biomass residues (leaves, fronds, trunks, empty fruit bunches, shells and fibers) constitute biomass waste produced from oil palm industries which is in abundance in south-east Asia (Chavalparit et al., 2006) (around 73.74 million tonnes per year in Malaysia (Rafatullah et al., 2013)). A common practice in managing oil palm residues is burning which give rise to environmental issues. Furthermore, it is composed of high carbon content (about 18 wt %) (Rafatullah et al., 2013), and could be the potential source for the production of carbon-based material for supercapacitor electrode construction.

EDLCs materials possess good stability but provide with the limited specific capacitance. On the other hand, PCs materials possess good capacitive storage but at a cost of low stability. It is timely to develop a hybrid energy system comprising of both materials and investigating their synergetic effect towards capacitive storage.

1.4 OBJECTIVES OF RESEARCH

The objectives of this research are:

1. To determine the physical and chemical characteristics of supercapacitor electrode materials such as MnO₂, reduced graphene oxide, carbon nanoparticles and reduced graphene oxide/MnO₂ nanocomposite.
2. To evaluate the electrochemical characteristics of MnO₂ recovered from spent batteries as supercapacitor electrode.
3. To evaluate the electrochemical characteristics of reduced graphene oxide from graphite source and porous carbon nanoparticles from biowaste (oil palm leaves) as supercapacitor electrodes.
4. To investigate the synergetic effect of carbon-based nanomaterials and MnO₂ towards enhanced energy storage properties.

1.5 SCOPE OF THE THESIS

The following research activities are required to achieve the mentioned objectives:

1. Recover MnO₂ from spent batteries through electrochemical method and produce MnO₂ with different electrochemical approaches.
2. Synthesize reduced graphene oxide nanosheets via modified Hummers' method and produce carbon nanoparticles from oil palm leaves via thermal annealing.
3. Synthesize reduced graphene oxide/MnO₂ nanocomposite through electrochemical method.
4. Study the structural properties of the synthesized materials with X-ray diffraction, UV spectroscopy, infrared spectroscopy, electron microscopy, N₂ adsorption-desorption and Raman spectroscopy.
5. Study the electrochemical properties of the synthesized materials with cyclic voltammetry, galvanostatic charge discharge and electrochemical impedance spectroscopy.
6. Fabricate the supercapacitor device with the synthesized materials and evaluate its long term stability.

CHAPTER 1

INTRODUCTION

1.1 CHAPTER OVERVIEW

This chapter introduces the basic aspects about the materials used in this study and background for the energy storage properties of the materials. Motivation of the research, problem statement, research objectives and scope of work are also presented in this chapter.

1.2 BACKGROUND AND MOTIVATIONS

Electrochemical capacitors (ECs) are also known as ultracapacitors or supercapacitors. It can be classified into two main categories based on energy storage mechanism, pseudocapacitors (PCs) and electrochemical double-layer capacitors (EDLCs). PCs store electrical energy faradically by electron charge transfer between electrode and electrolyte. Metal oxides and conducting polymers are used as electrode materials for PCs. In EDLCs, a double layer of electrolyte ions is formed on the surface of an electrode material, which arises from the potential-dependence of the surface density of charges stored electrostatically. The electrode materials for EDLCs include all carbon-based materials. Supercapacitors could be used in many applications because of

their higher energy output as compared to conventional capacitors and higher power than batteries, in addition to their miniature size. Various types of electrode materials can be used in supercapacitors, including carbon-based materials, conducting polymers and metal oxides. In addition, the electrolyte could be an aqueous, organic or an ionic liquid. In case of an aqueous electrolyte, the operating voltage is limited to 1 V (due to the electrochemical decomposition of water at 1.23 V), whereas an organic electrolyte can achieve a voltage range of 2.5 to 3.5 V (Syzdek et al., 2014). A higher voltage of up to 4.0 V can be achieved for the ionic liquid. Supercapacitors have many advantages, for example, long life cycles, fast charging time, low impedance and high energy and power density, environmental friendly, and also can be operated in a wide temperature range. This study aims to investigate different materials for supercapacitor applications with high power and long life criteria for better energy storage devices. The energy storage properties are directly depending on the structure and morphology of the electrode materials.

In recent years, manganese dioxide (MnO_2) has drawn increasing attention for supercapacitors application, mainly due to the high abundance of manganese (Jang et al., 2012) that contributes to low material cost as compared to the expensive ruthenium metal. Pang et al. reported high specific capacitance (C_s) (700 F g^{-1}) for MnO_2 thin films in year 2000 and their findings had sparked strong interest among energy research community for its application in supercapacitor electrode (Pang and Anderson, 2000, Pang et al., 2000). Such high capacitance value arises from the ions insertion/desertion within MnO_2 structure and it depends crucially on the particle size, surface area and porosity. Since then, in achieving optimized condition for the aforementioned properties, MnO_2 with different morphologies have been developed, such as nanoflakes (Chou et al., 2006), nanorods (Yousefi et al., 2012a), nanowires (Yousefi et al., 2013), nanopetals (Yang et al., 2012) and nanosheets (Yan et al., 2012). The synthesis route plays a vital role in determining its morphology. The most common synthesis route for MnO_2 is chemical coprecipitation method (Deng et al., 2013, Jiang et al., 2009) involving dissolved Mn^{4+} precursor. However, instability of Mn^{4+} precursor in the aqueous solution as well as the contact resistance between synthesized MnO_2 and current collectors have hindered its wider use in electrochemical applications (Xu et al., 2008, Prasad and Miura, 2004).

Electrochemical deposition is proven to be an effective method to prepare MnO₂ nanostructures (Hu et al., 2014, Yousefi et al., 2013).

On the other hand, carbon-based materials possessing high surface area as the electrode material, and the capacitance originates from the charge accumulation at the interface between electrode and electrolyte (Portet et al., 2005). Pseudocapacitors employ transition metal oxides or conductive polymers (Patil et al., 2013, Song et al., 2013, Xie et al., 2012) as the electrode material. Though the energy densities in pseudocapacitors are higher than that of EDLCs, the faradic reactions within pseudocapacitors could lead to phase changes and limit their life time (Compton and Nguyen, 2010). Graphene with its high surface area and nanosheets morphology and carbon nanoparticles with porous structure are a promising materials from energy storage applications.

1.3 PROBLEM STATEMENT

The need for the development of efficient energy storage systems is paramount in meeting the world's future energy targets, especially when the energy costs are on the increase in addition to the escalating demand. Energy storage technologies can improve efficiencies in supply systems by storing the energy when it is in excess, and then release it timely. Nowadays, batteries are slowly becoming obsolete due to their poor cycleability (limited to a few thousands) and long charge time (tens of minutes) in comparison to supercapacitors. On the other hand, supercapacitors have long life time and fast charging times (Vangari et al., 2013). Nowadays the research focus on developed suitable electrode materials which directly reflect in supercapacitor technology enhancement.

MnO₂ has been identified as a promising pseudocapacitive material to replace toxic and costly materials especially ruthenium oxide. Though manganese source can be found abundantly in nature, it is imperative to stop exploiting nature for the advancement of technology. Instead, recovery of manganese from waste sources could be an alternative to obtain MnO₂. According to United States Environmental Protection Agency (USEPA) analysis, an average of 8 disposable batteries are consumed by an individual annually.

CHAPTER 3

EXPERIMENTAL PROCEDURES AND TECHNIQUES

3.1 CHAPTER OVERVIEW

Detailed information about samples preparation for the present research are given in this chapter. The prepared materials for this study are MnO₂, reduced graphene oxide, carbon nanoparticles and reduced graphene oxide/MnO₂ nanocomposite. In addition, this chapter shows a background about chemical and physical characterization techniques, in order to study the properties of the prepared materials such as XRD, FTIR, TGA/DTA, FESEM, TEM, Raman, UV–Vis and N₂ adsorption–desorption techniques. Finally, the electrodes preparation and cells setup used for supercapacitive testing are mentioned in details.

3.2 SAMPLES PREPARATION PROCEDURES

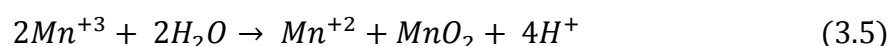
3.2.1 Preparation of MnO₂ from Recycling of Spent Batteries

A spent Zn–C battery (EVEREADY® D cell) was disassembled and the cathode black paste was taken and used for the subsequent process. The cathode black paste was dried at 130 °C for 24 hours, ground well in a mortar, and then was sieved using 200 μm

mesh. The sieved powder was later washed with deionized water (solid to liquid ratio 1:10) in order to remove NH_4Cl electrolyte from the cathode past in the battery and finally dried at $105\text{ }^\circ\text{C}$ for 24 hours. The dried powder (20 g) was subsequently dissolved in H_2SO_4 (200 mL, 2 M, Friendemann Schmidt), followed by addition of $\text{H}_2\text{C}_2\text{O}_4$ (14.5 g, Aldrich) which act as reducing agent. The leaching process was continued with continuous stirring for 5 hours at $80\text{ }^\circ\text{C}$ (Rácz and Ilea, 2013, Ferella et al., 2008). The reactions which were involved in this preparation are summarized as shown below:



The leached solution was filtered prior to electrowinning. For electrowinning, two stainless steel plates were set up as electrodes and the distance between electrodes was kept at 20 mm. Electrowinning was carried out in 50 mL of leached solution with current density of 0.15 A cm^{-2} for 1 hour at room temperature. Electrowinning involves Mn(II) oxidation to Mn(III) and followed by disproportionation to Mn(II) and Mn(IV). MnO_2 was then formed as dark precipitate at the bottom of the cell. $\text{MnO}_2(\text{Bt})$ was used as a code for the prepared material. The reaction mechanism can be described as follows (Souza and Tenório, 2004):



3.2.2 Preparation of MnO₂ by Potentiostatic and Galvanostatic Electrodeposition

MnO₂ was electrodeposited from KMnO₄ solution (0.5 M, Aldrich) by potentiostatic and galvanostatic techniques by applying 10 V and 0.165 A cm⁻² for 30 minutes at room temperature, respectively. Two pre-treated stainless steel plates were used as electrodes. The distance between two electrodes was kept constant at 20 mm throughout the electrodeposition process. For both electrodeposition techniques, black films were obtained on the cathode and the mass was recorded after drying. MnO₂(PS) and MnO₂(GS) were used as codes for the prepared materials by potentiostatic and galvanostatic techniques, respectively.

3.2.3 Preparation of Reduced Graphene Oxide Nanosheets

Graphene oxide (GO) was prepared from graphite by Hummers' method (Hummers and Offeman, 1958). In order to prevent incomplete oxidation, graphite powder was pre-oxidized by slowly mixed and stirred with graphite (20 g, Merck), K₂S₂O₈ (10 g, Aldrich) and P₂O₅ (10 g, Aldrich) into concentrated H₂SO₄ (30 mL). The reaction mixture was heated up to 80 °C using an oil bath and continuous stirring for 6 hours. The mixture was then diluted with distilled water, filtered and washed until the filtrate became neutral in pH condition. The washed powder was dried for 8 h in a vacuum oven at 60 °C. The pre-oxidized graphite powder was oxidized as follows: the pre-oxidized graphite powder was added to concentrated H₂SO₄ (460 mL) cooling in an ice bath. KMnO₄ (60 g) was added to the pre-oxidized solution and continuously stirred over 30 minutes. The mixture was then heated up to 35 °C for 2 hours before distilled water (1 L) was added. The stirring was continued for 15 minutes and additional distilled water (3 L) and 30 % H₂O₂ (50 mL, Merck) were added onto the mixture. The mixture was then filtered, washed with aqueous HCl (1:10, Merck) and dried in vacuum oven at 60 °C in order to obtain dry graphite oxide. Exfoliation of graphite oxide was done by sonicating graphite oxide dispersion (2 g L⁻¹) at 200 W for 30 minutes. The dispersion was later centrifuged at 6000 rpm for 10 minutes to remove the